
Article

Not peer-reviewed version

Mathematical Modelling of Virus Spreading in COVID-19

[Liaofu Luo](#) * and [Jun Lv](#) *

Posted Date: 14 July 2023

doi: 10.20944/preprints202307.0965.v1

Keywords: virus spread; COVID-19; mathematical model; daily number of infections; cumulative number of infections



Preprints.org is a free multidiscipline platform providing preprint service that is dedicated to making early versions of research outputs permanently available and citable. Preprints posted at Preprints.org appear in Web of Science, Crossref, Google Scholar, Scilit, Europe PMC.

Copyright: This is an open access article distributed under the Creative Commons Attribution License which permits unrestricted use, distribution, and reproduction in any medium, provided the original work is properly cited.

Article

Mathematical Modelling of Virus Spreading in COVID-19

Liaofu Luo ^{1,*} and Jun Lv ^{2,*}

¹ Faculty of Physical Science and Technology, Inner Mongolia University, 235 West College Road, Hohhot 010021, China; lolfc@imu.edu.cn

² College of Science, Inner Mongolia University of Technology, 49 Aymin Street, Hohhot 010051, China; lujun@imut.edu.cn

* Correspondence: lolfc@imu.edu.cn (L.L.); lujun@imut.edu.cn (J.L.); Tel.: +86-471-4992676 (L.L.); +86-13039500654 (J.L.)

Abstract: A mathematical model is proposed to analyze the spreading dynamics of COVID-19. By using the parameters of the model, namely the basic reproduction number (R_0) and the attenuation constant (k), the daily number of infections (DNI) and the cumulative number of infections (CNI) are deduced and shown to be in good agreement with experimental data. This model effectively addresses three key issues: explaining the waveform pattern of DNI, predicting the occurrence of the second wave of infection, and understanding the competitive spread of two viruses in a region. The findings demonstrate that these significant challenges can be comprehensively tackled using a simple mathematical framework. The theoretical insights derived from this model hold potential in guiding the estimation of the severity of an infection wave and formulating effective strategies for the control and mitigation of epidemic outbreaks.

Keywords: virus spread; COVID-19; mathematical model; daily number of infections; cumulative number of infections

1. Introduction

The ongoing COVID-19 pandemic has posed several unresolved questions. Firstly, our aim is to understand the reason behind the waveform pattern observed in the Daily Number of Infections (DNI) and to predict the scale and duration of an infection wave, including the Cumulative Number of Infections (CNI) and the time for infection ending. Secondly, we investigate why the second wave of infection typically follows the first wave and how to predict its occurrence. Lastly, we explore how virus spreading in a region is influenced by the emergence of new strains and develop methods to control their spread. Existing epidemic models have limitations in addressing these problems comprehensively. Firstly, since the 1920s the differential equations were used to model the population distribution of disease spread, including susceptible, infected, and recovered/dead pools [1,2]. Such models could not examine important social and behavioural factors, such as the behavioural responses of individuals to policy measures, and the effect of heterogeneous social contacts on diffusion patterns. Secondly, since the 1990s agent-based simulations were proposed that include some important sources of population heterogeneity and explore the structure and dynamics of transmission networks. However, none of the agent-based models are based on explicit empirical/theoretical assumptions of individual behaviour, social transmission mechanisms and social structure constraints [3-5]. Recently, several network models simulating the spread of epidemics in the population were proposed, such as the Susceptible-Infectious-Susceptible model on random networks [6], and the epidemic spreading on modular networks [7]. Although these specific models have solved some aspects of the complexity of infectious diseases and obtained meaningful results, they still fail to comprehensively answer the aforementioned unresolved questions.

As the Chinese idiom goes, "The greatest truths are the simplest". Starting from the principle of natural selection - the interaction and compromise between the virus and its host (human) - we

propose a mathematical model based on insights from experimental data. The model is based on two fundamental assumptions. First, each viral strain has a basic reproduction number (R_0), which represents the average number of infections caused by an initial infectious person in a completely susceptible population [8]. R_0 is a measure of the transmission potential of a particular infectious disease. Second, virus infections undergo a series of events in m steps that weaken with each step, described by an attenuation constant k ($k < 1$). The parameter k is influenced by social contacts and policy measures, where looser contacts and measures result in higher values of k . Based on two parameters R_0 and k we can deduce the general formula for the Daily Number of Infections (DNI) and the Cumulative Number of Infections (CNI) over m steps. The CNI is denoted by $F(R_0, k; m)$. These formulas are in good agreement with experiments and provide a generalized framework to simulate single and multiple virus infections. By introducing F_1 and F_2 we can also study the competitive spread of two viruses in a region, including scenarios with the introduction of a new virus strain. It is worth noting that the loosening of public health measures and/or the emergence of new viruses can lead to subsequent waves of virus transmission.

2. Materials and Methods

The data of daily virus infections of COVID-19 are taken from WHO (<https://covid19.who.int/data>) for the UK and from the public database (<https://ourworldindata.org/coronavirus>) for Hong Kong. Since Gauss discovered the least square method and successfully applied it to astronomical observation, the ordinary Least Square is recognized as one of the best methods for curvilinear regression. In the present study, we use the Least Square simulation of observational data of the virus infection to determine the parameters in each COVID-19 pandemic. The goodness of the nonlinear Least Square fitting (NLLSF) is tested by R^2 , i.e.

$$R^2 = 1 - \frac{\sum_{i=1}^n (y_i - \hat{\pi}_i)^2}{\sum_{i=1}^n (y_i - \bar{y})^2},$$

where y_i are the observation values, \bar{y} their average and $\hat{\pi}_i$ the predictions of the model. The goodness R^2 and the p-value of Prob(F-statistic) are calculated for each simulation. Define F-statistic as

$$F - \text{statistic} = \frac{(\sum_{i=1}^n (y_i - \bar{y})^2 - \sum_{i=1}^n (y_i - \hat{\pi}_i)^2)/(k-1)}{\sum_{i=1}^n (y_i - \hat{\pi}_i)^2/(n-k)},$$

(n – number of samples, v - number of parameters) that can be calculated from the experimental data. The p-value is decided by the percentile of the Fisher's F-distribution $F_{v-1, n-v}(z)$, namely,

$$\text{p - value} = \text{the probability of } F_{v-1, n-v}(z) > F - \text{statistic}.$$

The goodness R^2 , the p-value and the root mean squared error (RMSE) for each simulation are given in the figures.

3. Results

3.1. Derivation of formulas for Cumulative Number of Infections (CNI) and Daily Number of Infections (DNI)

The potential for infection of a given virus strain is determined by the basic reproduction number known as R_0 . For the virus to spread, it must continually re-infect the host population. However, countermeasures by humans must aim to limit these subsequent infections. Essentially, this implies that the interaction and compromise between the virus and host (humans) necessitates the j -th reproduction number R_j to be smaller than the $(j-1)$ -th reproduction R_{j-1} , as expressed in the equation

$$R_j = kR_{j-1}, (k < 1).$$

The attenuation constant ' k ' in this scenario is influenced by social contact rates and policy measures. After $m-1$ rounds of infection spread, the total number of infections in a specific area can be represented as

$$F(R_0, k; m) = R_0 + R_0 R_1 + \dots + R_0 R_1 R_2 \dots R_{m-1} = R_0 + k R_0^2 + \dots + k^{m(m-1)/2} R_0^m. \quad (1)$$

This function $F(R_0, k; m)$ describes the Cumulative Number of Infections (CNI), which is an increasing function of m . Assuming the total infected individuals as N , solving the equation $F(R_0, k; m) = N$ will produce ' m ', the transmission number of the virus strain. The parameter m grows with time t . Assuming each transmission takes place every q days, we have

$$m = (t + t_0)/q, \quad (2)$$

where t_0 is a time shift parameter linked to the start of infection (the time of $m=1$). Inserting (2) into (1) we obtain a formula of CNI vs t represented by four parameters R_0 , k , q and t_0 that can be used to simulate the change of a cumulative number of infections with time in a region. As seen in Figure 1, our simulations of the UK-alpha strain (November 2020 to April 2021) and the Hong Kong-delta/omicron strain (February 2022 to April 2022) spreading are well fitted to the data obtained from COVID-19 pandemic updates.

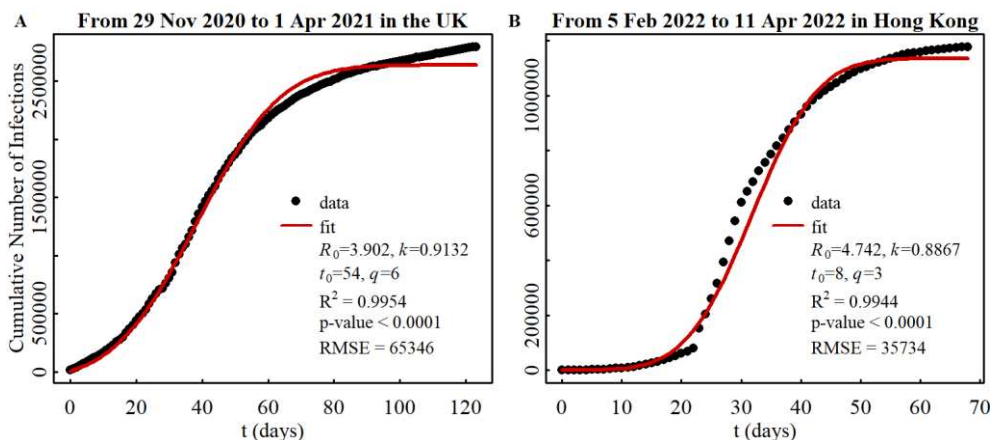


Figure 1. COVID-19 pandemics in the UK (A) and Hong Kong (B).

Applying Equations (1) and (2), the Daily Number of Infections (DNI) is derived:

$$\begin{cases} dF/dt = (dF/dm)/q \\ dF/dm = k^{m(m-1)/2} R_0^m. \end{cases} \quad (3)$$

From Eq (3), it is easy to understand why DNI first rises then falls, considering that $R_0 > 1$ (for most infectious viruses) and $k < 1$. Zero DNI is arrived when $dF/dm = 0$, which requires m to be large enough such that

$$k^{(m-1)/2} R_0 < 1 \text{ or } R_0 < (1/k)^{(m-1)/2}. \quad (4)$$

This is a condition for the end of an infection wave.

3.2. Insights from typical figures of CNI vs m

Utilizing Eq (1), we plotted the change of CNIs with variables k and m for the given R_0 (Figure 2). Figures 2A-E show typical cases that help in understanding the development and termination of an infection wave.

From Figure 2, one can observe that the curve of $F(R_0, k; m)$ increases with m and approaches a stable value when $m > m_{st}$ for each $k < k_{th}$. We denote $F(R_0, k_{th}; m_{st})$ as N_{th} . Calculating for $m_{st} = 15$ in Figure 2A to 2E, we obtained the threshold k_{th} and the corresponding CNI, N_{th} , for each given R_0 (each virus strain). On the other hand, CNI attaining a stable value means DNI approaching zero. By defining

$E_{km} = (1/k_{th})^{(m_{st}-1)/2}$ Eq (4) can be written as $R_0 < E_{km}$. The threshold k_{th} , the corresponding CNI N_{th} and the parameter E_{km} are listed in Table 1. We found the relation $R_0 < E_{km}$ to hold well across all data.

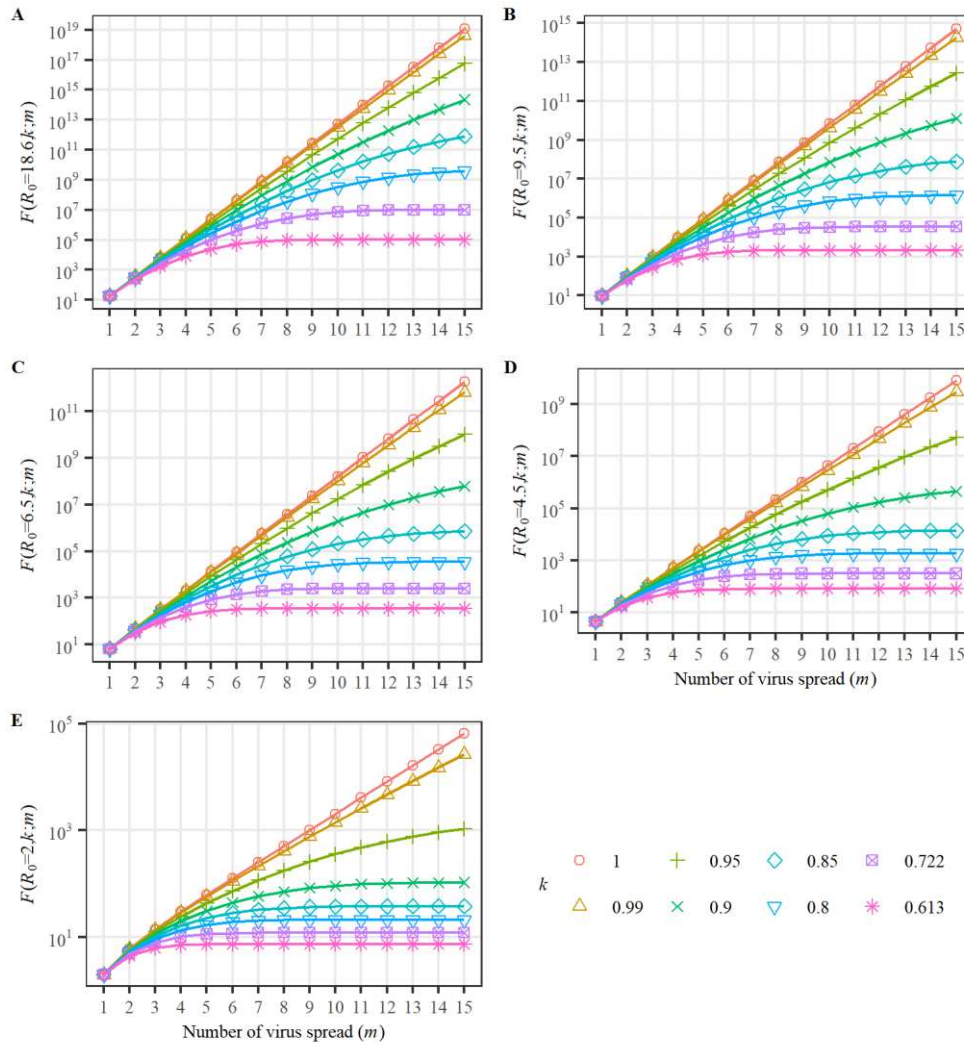


Figure 2. CNI functions $F(R_0, k; m)$ for several typical R_0 values. Panel A: $R_0=18.6$ (for Omicron BA.4, BA.5 in South Africa, 2022-1), panel B: $R_0=9.5$ (for Omicron B.1.1.529 in many countries, 2021-11), panel C: $R_0=6.5$ (for Delta in India, $R_0=5-8$, 2020-10), panel D: $R_0=4.5$ (for Alpha in the UK, 2020-9, Beta in South Africa, 2020-5, Gamma in Brazil, 2020-11, $R_0=4-5$), and panel E: $R_0=2$ (for SARS-CoV 2003, $R_0=2-3$).

Table 1. Parameters related to virus infection dying out.

R_0	$k_{th}(m_{st}=15)$	$E_{km}=(1/k_{th})^7$	N_{th}	$k_{cr}(N_{max}=10^7)$
18.6	0.613	30.7	10^5	0.722
9.5	0.722	9.78	$\sim 10^5$	0.8
6.5	0.75	7.49	$\sim 10^4$	0.85
4.5	0.8	4.77	$\sim 10^3$	0.9
2	0.9	2.09	$\sim 10^2$	>0.95

The daily increasing number $dF/dm=0$ means the virus infection dies out. The above result shows the higher the basic reproduction number R_0 , the more strict public health measure is required to increase E_{km} to satisfy Eq (4) and terminate the wave of virus infection effectively. From Table 1 we found the cumulative infection numbers N_{th} of many virus strains (except Omicron with $R_0=18.6$) are lower than 10^5 if appropriate k (lower than k_{th}) is introduced.

For the virus strain of given R_0 , if $F(R_0, k; m)$ (for all m) exceeds a threshold N_{\max} , then the spread of this strain would lead to a wave of COVID-19 pandemic in a region with population larger than N_{\max} . In order to end this spread, the necessary condition would be

$$F(R_0, k; m) < N_{\max} \quad (\text{for all } m). \quad (5)$$

Equation (5) provides a constraint on k for strains with R_0 . The critical value of k is denoted as k_{cr} . Taking $N_{\max} = 10^7$ the values of k_{cr} are also listed in Table 1. Note that the parameter k_{th} is the threshold value of k required for ending the spread in 15th generation, but the parameter k_{cr} is that value for ending the spread in arbitrary generation. The latter constraint is looser than the former. Therefore, k_{cr} is larger than k_{th} .

Virus strains with low R_0 values have higher k_{cr} and k_{th} values. As a result, they can spread in regions with smaller populations under looser public health measures. This theoretical prediction can explain why strains like SARS-CoV in 2003 only spread in restricted regions and soon disappeared globally. On the contrary, virus strains with high R_0 values, such as Omicron, have lower k_{cr} and k_{th} values. To satisfy Equations (4) and (5), the parameter k needs to meet very strict constraints. In cases where social management measures are not stringent enough, the number of infected individuals will quickly surpass the N_{\max} limit, triggering a global pandemic wave, possibly culminating in a type of coexistence between viruses and humans.

In summary, the termination of an infection wave is determined by the condition $dF/dm = 0$ on the CNI diagram (Figure 2), which requires a sufficiently large m and the condition in Equation (4) satisfied, i.e. $R_0 < E_{km} = (1/k_{\text{th}})^7$. Additionally, the necessary condition for a pandemic to die out in a population of N_{\max} is expressed by Equation (5), imposing a limitation on k , namely $k < k_{\text{cr}}$.

3.3. Prediction on the second wave of pandemics

Early models based on previous pandemics such as SARS, MERS, and the 2009 H1N1 outbreak can effectively predict the occurrence of the first wave of a disease. However, their predictive power decreases when it comes to anticipating the possibility of a second wave [9]. This raises the question: Why does the second wave of COVID-19 infections often follow the first wave? The present model aims to address this issue.

As shown in Figure 2, there are multiple curves (F versus m) for a given R_0 value. These curves differ from each other by the parameter k . When the number of daily new infections (DNI) approaches zero, any fluctuation in k significantly influences the spread of the virus. Therefore, changes in public health measures can induce variations in virus spread along different curves. Generally, as public health measures are relaxed, the parameter k increases, causing the virus to transition from one curve of F to another steeper curve. This signifies the onset of a new wave of virus spread. For instance, in Figure 2A, the spread of the Omicron variant (with an R_0 of 18.6) is plotted. Assuming the initial spread is along the curve with k equal to 0.613, a stable state is reached at $m=15$. At this point, the k value increases to 0.722. In response to this change, the virus begins spreading along a new curve with $k=0.722$, starting from $m=4$, as the value of $F(18.6, 0.722; m=4)$ is equal to the original CNI value, $F(18.6, 0.613; m=15)$. This example explains how the second wave of virus infection occurs. However, in cases where the parameter k decreases when DNI approaches zero, the curve of F will transition to a flatter one. This indicates that the first wave of viral infection will end soon and no second wave will occur.

By examining Figure 2A to Figure 2E, we can analyze how the occurrence of a second wave depends on the R_0 value of the virus. For instance, as k changes from 0.85 to 0.9, the CNI (at $m=15$) for high R_0 viruses increases hundreds of times, whereas it only increases tens of times for low R_0 viruses. Therefore, our model predicts that multi-wave infections are more likely to occur with viruses that have high R_0 values.

In the aforementioned discussions, we have assumed that no virus mutation occurs and that only one type of virus is spreading. In reality, changes in public health measures may be accompanied by virus mutations. In this case, the change in public health measures would cause the jump of F not

only between different curves with a given R_0 but also between different R_0 values, providing more opportunities for the occurrence of a second wave during virus spread.

Another crucial point to consider is that the change in k can simultaneously induce a change in q , as the eigen-time (inherent time) m depends on q (Equation (2)). In the case of a single wave, the parameter m can be used to represent time dependence, and q can be simply set to 1 (known as normalization). However, when studying two continuous waves, the dependence on q should be clearly indicated due to the different eigen-times m . We have mentioned that the dependence of F on the change in k results in a jump from one curve to another. Meanwhile, the dependence of F on the change in q only affects the lengthening or shortening of the abscissa of the graph without altering the shape of the curve. When the public health measures change and a jump between curves occurs, the abscissa of the graph of the second wave simultaneously lengthens or shortens.

The occurrence of the second wave of infection is more likely when public health measures are relaxed. This change in the second wave is accompanied by a change in the q value. These predictions align with experimental data. For example, in the UK from May to September 2021, public health measures were relaxed, and a second wave of infection followed the first wave (Figure 1A). Similarly, in Hong Kong several months after May 2022, the looser public health measures led to a second wave occurring after the first wave (Figure 1B). (The data on the change of public health measures can be found at <https://www.bsg.ox.ac.uk/research/covid-19-government-response-tracker>)

In summary, the dependence of CNI on k (given a specific R_0) is determined by the jump between different curves on the graph $F(R_0, k; m)$ versus m , referred to as k -transformation. The dependence of CNI on the duration of m is obtained by stretching the abscissa m on the graph, known as q -transformation. The k -transformation and q -transformation, occurring when the first wave is nearing its end, are the causes of a continuous second wave. The change in k is attributed to the modification of public health measures, while the modification of q is due to the change in physical time within a unit of m . The changes in k and q provide an explanation for the experimental data on continuous multi-wave infections.

3.4. Cross-spread of two viruses: Discriminant function

Viral infections often involve the simultaneous presence of two or more viruses. To accurately simulate the cross-spread of two viruses, it is necessary to consider the differences in eigen-times (m_1 and m_2) between these viruses and their relationship with the physical time t . Consequently, additional parameters q and t_0 (as given in Eq (2)) must be taken into account. By utilizing the four parameters R_0 , k , q and t_0 , the CNI $F(R_0, k; m)$ can be expressed as:

$$F(R_0, k; m(t)) = F(t; a, b, c, d), (a = R_0, b = k, c = q, d = t_0). \quad (6)$$

When the CNIs of two virus strains $F_1(t; a_1, b_1, c_1, d_1)$ and $F_2(t; a_2, b_2, c_2, d_2)$ intersect at t_{cr} ,

$$F_1(t_{\text{cr}}; a_1, b_1, c_1, d_1) = F_2(t_{\text{cr}}; a_2, b_2, c_2, d_2), \quad (7)$$

and

$$\begin{cases} F_1(t; a_1, b_1, c_1, d_1) > F_2(t; a_2, b_2, c_2, d_2) & (t < t_{\text{cr}}) \\ F_1(t; a_1, b_1, c_1, d_1) < F_2(t; a_2, b_2, c_2, d_2) & (t > t_{\text{cr}}) \end{cases}$$

This represents a transition in the population of virus strains from F_1 to F_2 . As it is challenging to directly solve the intersection equation (Eq (7)), we introduce a function:

$$D_{21} = \log[(dF_2/dt)/(dF_1/dt)], \quad (8)$$

which satisfies:

$$\begin{cases} D_{21} > 0 & \text{as } dF_2/dt > dF_1/dt \\ D_{21} < 0 & \text{as } dF_2/dt < dF_1/dt \end{cases} \quad (9)$$

By utilizing Eqs (2)(3)(6) and (8) D_{21} can be formulated as a simple quadratic function of time

$$D_{21} = \alpha t^2 + \beta t + \gamma, \quad (10)$$

where

$$\begin{cases} \alpha = \log b_2/(2c_2^2) - \log b_1/(2c_1^2) \\ \beta = (2d_2 - c_2)\log b_2/(2c_2^2) - (2d_1 - c_1)\log b_1/(2c_1^2) + \log a_2/c_2 - \log a_1/c_1 \\ \gamma = d_2(d_2 - c_2)\log b_2/(2c_2^2) - d_1(d_1 - c_1)\log b_1/(2c_1^2) + d_2\log a_2/c_2 - d_1\log a_1/c_1 + \log(c_1/c_2) \end{cases}$$

In order to determine if a real root of D_{21} exists, we define:

$$\Delta = \beta^2 - 4\alpha\gamma. \quad (11)$$

The value of Δ determines the existence of the real root in the quadratic form D_{21} . This form, known as the discriminant function, serves as a tool to identify the occurrence of t_{cr} and the domain of its existence. The prediction rules can be summarized as follows:

Rule 1: When $\Delta > 0$, the quadratic form intersects with t axis at t_s and t_m ($t_m > t_s$),

$$t_s = \begin{cases} \frac{-\beta - \sqrt{\Delta}}{2\alpha} & (\text{for } \alpha > 0) \\ \frac{-\beta + \sqrt{\Delta}}{2\alpha} & (\text{for } \alpha < 0) \end{cases}, \quad t_m = \begin{cases} \frac{-\beta + \sqrt{\Delta}}{2\alpha} & (\text{for } \alpha > 0) \\ \frac{-\beta - \sqrt{\Delta}}{2\alpha} & (\text{for } \alpha < 0) \end{cases}.$$

These values partition the time into three distinct domains: $t < t_s$ in the first domain, $t_s < t < t_m$ in the second domain and $t > t_m$ in the third domain.

Rule 2: In the first domain, $t_a = qm_0 - t_0$ is defined as the initial time where $m_0 \gg 1$, indicating $m_{1,2} = (t + d_{1,2})/c_{1,2} \gg 1$. If $D_{21} > 0$, there will be no intersection of $F_1(t)$ and $F_2(t)$ in the domain between t_a and t_s when the initial values of F at t_a satisfy $F_1(t_a) < F_2(t_a)$, but there may be one t_{cr} (the number of t_{cr} is either 1 or 0) in the domain when $F_1(t_a) > F_2(t_a)$. If $D_{21} < 0$, there will be no intersection of $F_1(t)$ and $F_2(t)$ in the domain when the initial values satisfy $F_1(t_a) > F_2(t_a)$, but there may be one t_{cr} (the number of t_{cr} is either 1 or 0) when $F_1(t_a) < F_2(t_a)$.

Rule 3: In the second domain, if $D_{21} > 0$ there will be no intersection of $F_1(t)$ and $F_2(t)$ in the domain when the F -values at $t = t_s$ satisfy $F_1(t_s) < F_2(t_s)$, but there may be one t_{cr} (the number of t_{cr} is either 1 or 0) when $F_1(t_s) > F_2(t_s)$. If $D_{21} < 0$ there will be no intersection of $F_1(t)$ and $F_2(t)$ in the domain when the F -values at $t = t_s$ satisfy $F_1(t_s) > F_2(t_s)$, but there may be one t_{cr} (i.e. the number of t_{cr} is either 1 or 0) when $F_1(t_s) < F_2(t_s)$. The F -values at $t = t_s$ are determined by $F_1(t)$ and $F_2(t)$ in the first domain.

Rule 4: In the third domain, if $D_{21} > 0$ there will be no intersection of $F_1(t)$ and $F_2(t)$ in the domain when the F -values at $t = t_m$ satisfy $F_1(t_m) < F_2(t_m)$, but there may be one t_{cr} (the number of t_{cr} is either 1 or 0) when $F_1(t_m) > F_2(t_m)$. If $D_{21} < 0$ there will be no intersection of $F_1(t)$ and $F_2(t)$ in the domain when the F -values at $t = t_m$ satisfy $F_1(t_m) > F_2(t_m)$, but there may be one t_{cr} (i.e. the number of t_{cr} is either 1 or 0) when $F_1(t_m) < F_2(t_m)$. The F -values at $t = t_m$ are determined by $F_1(t)$ and $F_2(t)$ in the second domain.

Rule 5: There can be at most one t_{cr} in a given domain because the symbol of D_{21} is definite in any domain. The magnitude of the domain is an important factor to predict the occurrence of a t_{cr} . For example, in the second domain the magnitude is $t_m - t_s = \Delta^{1/2}/(2|\alpha|)$, and the necessary condition for the occurrence of t_{cr} is a large enough $(t_m - t_s)$ or Δ .

Rule 6: When $\Delta < 0$, the quadratic form D_{21} does not intersect with t axis. In this case, there is only one domain and the rule is the same as that in the first domain given by Rule 2.

Figure 3 presents examples of cross-spread of two virus strains, 1 and 2. The left panel shows the discriminant function, and the right panel displays the cross-spread of the two strains. The influence of the change in parameters (as an example, we only assume the R_0 value of strain 1 changes) on the intersection of two strains is shown in the figure. In Figure 3A, there is no intersection. In Figure 3B and 3C, there are two intersections in the second and third domain, respectively. In

Figure 3D, there is one intersection in the second domain. These intersection occurrences are in agreement with aforementioned prediction rules.

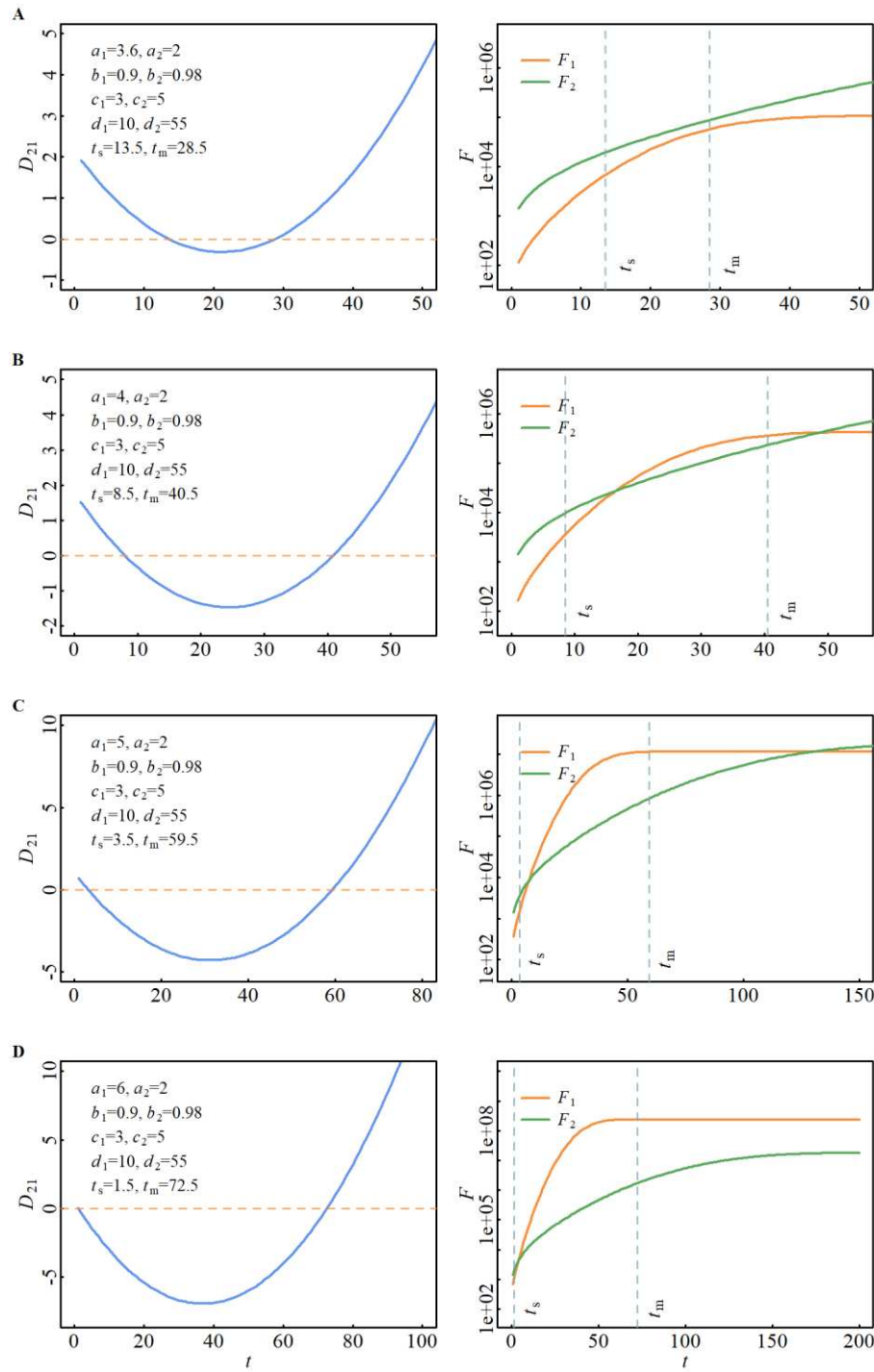


Figure 3. Discriminant Function and intersection occurrence.

In the first domain we have introduced $t_a = qm_0 - t_0$ as the initial time. To study the cross spread in the time interval between $m=1$ and t_a where dF/dt in D_{21} is difficult to be defined one should use $F(t)$ -ladder method as follows:

The step size of CNIs of the first few steps in two ladders 1 and 2 are given by $a_1, b_1 a_1^2, b_1^3 a_1^3, b_1^6 a_1^4, b_1^{10} a_1^5, b_1^{15} a_1^6, b_1^{21} a_1^7, b_1^{28} a_1^8, b_1^{36} a_1^9$, etc., and $a_2, b_2 a_2^2, b_2^3 a_2^3, b_2^6 a_2^4, b_2^{10} a_2^5, b_2^{15} a_2^6, b_2^{21} a_2^7, b_2^{28} a_2^8, b_2^{36} a_2^9$, etc., respectively (Eq (1)). Strain 1 spreads from the 1st step a_1 at $t=c_1-d_1$ on ladder 1 and strain 2

spreads from the 1st step a_2 at $t=c_2-d_2$ on ladder 2. The CNI and arrival time t of the two strains on their respective ladders are listed in Table 2. For example, let's take $c_1=7$, $d_1=15$, $c_2=5$, $d_2=10$. The earlier arrival times, in turn, are $t=c_1-d_1=-8$, $c_2-d_2=-5$, $2c_1-d_1=-1$, $2c_2-d_2=0$, $3c_1-d_1=6$, $3c_2-d_2=5$, etc. By using Table 2, one can easily calculate the CNI at each arrival time as the parameters a_1 , b_1 , a_2 , b_2 are given, compare the CNI values on two ladders and obtain the information on the cross spread of two strains.

Table 2. CNI and arrival time t of two strains on $F(t)$ -ladder.

t	CNI
c_i-d_i ¹	a_i
$2c_i-d_i$	$a_i+b_i a_i^2$
$3c_i-d_i$	$a_i+b_i a_i^2+b_i^3 a_i^3$
$4c_i-d_i$	$a_i+b_i a_i^2+b_i^3 a_i^3+b_i^6 a_i^4$
$5c_i-d_i$	$a_i+b_i a_i^2+b_i^3 a_i^3+b_i^6 a_i^4+b_i^{10} a_i^5$
$6c_i-d_i$	$a_i+b_i a_i^2+b_i^3 a_i^3+b_i^6 a_i^4+b_i^{10} a_i^5+b_i^{15} a_i^6$

¹ $i=1, 2$ refer to two strains respectively, to save space only six steps of the $F(t)$ -ladder are listed.

3.5. Examples of the cross-spread of two viruses

The epidemics that occurred in the UK from November 2020 to February 2022 provide a clear demonstration of the cross-spread phenomenon involving multiple viruses. This process can be divided into five stages, namely: (A) the alpha epidemic, (B) the delta invasion and cross-spread of two strains, (C) the delta dominant stage, (D) the omicron invasion and cross-spread of delta and omicron, and (E) the omicron dominant stage. In this section, we will specifically focus on studying the cross-spread of two strains during stage B and D.

Firstly, let us examine the cross-spread between the alpha strain (designated as strain 1) and the delta strain (designated as strain 2) during stage B. The spread of the alpha strain during stage A has been represented in Figure 1A, where we obtained the parameter $a_1=R_0^{(1)}=3.9$. The spread of the delta strain during stage C has been illustrated in Figure 4A, and we derived the parameter $a_2=R_0^{(2)}=5.1$ based on this data. By using $R_0^{(1)}$ and $R_0^{(2)}$ as inputs, we simulated the cross-spread of the two strains, as depicted in Figure 4B. Furthermore, utilizing all the parameters a_i , b_i , c_i , d_i ($i=1,2$) obtained from Figures 1A, 4A, and 4B, we constructed the discriminant function of the cross-spread and plotted the intersection of the two strains during stage B in Figure 4C. Interestingly, we discovered that one t_{cr} occurs at $t=71$ in the region where $t>t_m$ ($t_m=44.5$), which is consistent with the prediction outlined in **Rule 4**.

Similarly, we investigated the cross-spread between the delta strain (strain 1) and the omicron strain (strain 2) during stage D. The results of this analysis are shown in Figures 5A, 5B, and 5C. From Figure 5C, we observed that a t_{cr} appears at $t=42$ in the region where $t>t_m$ ($t_m=28.5$), which is in agreement with the prediction made by **Rule 4**.

In both simulations, we assumed April 1 as the initial time for stage B, and November 11 as the initial time for stage D. Due to the uncertainty surrounding the exact timing of the delta invasion in stage B and the omicron invasion in stage D, we shifted the initial times t of stages B and D by several days. Remarkably, we found that the same values of k_1 , k_2 , q_1 , q_2 , $t_0^{(1)}$ were obtained, and only $t_0^{(2)}$ varied while still maintaining the invariant $t+t_0^{(2)}$.

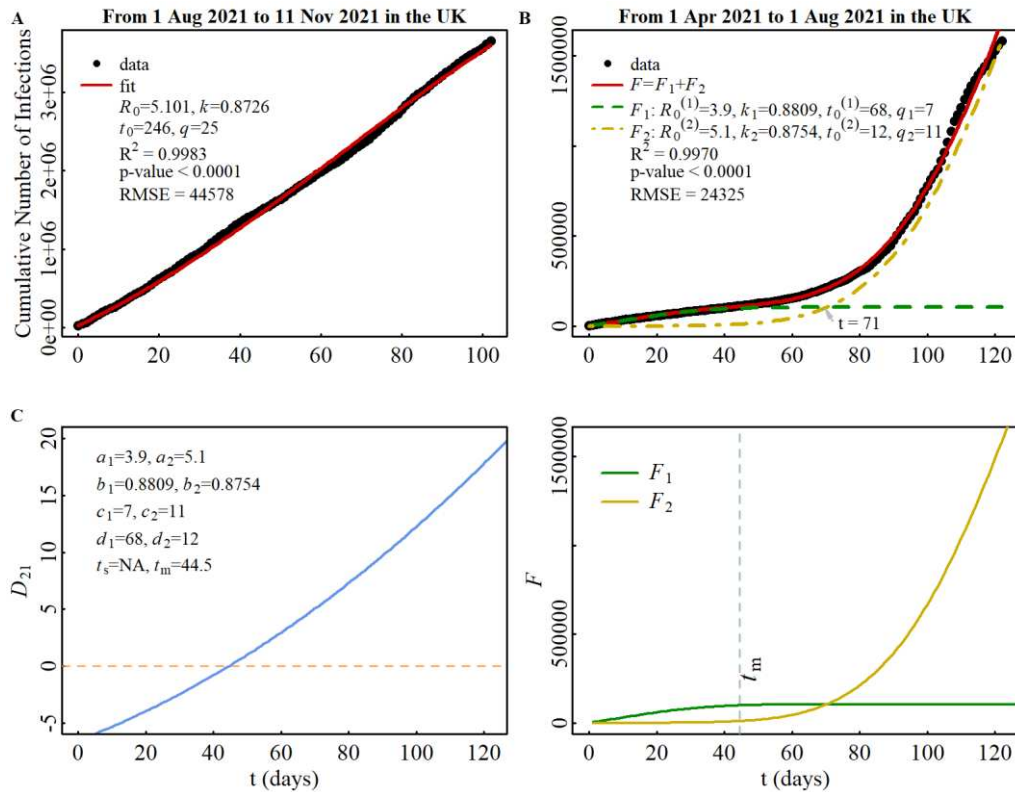


Figure 4. CNI simulation in the UK from November 2020 to November 2021. Panel A: CNI simulation of delta spread in stage C, panel B: CNI simulation of alpha/delta spread in stage B, and panel C: discriminant function and intersection of alpha/delta spread in stage B (left panel gives discriminant function and right panel the cross-spread of two strains). Note: CNI simulation of alpha spread in stage A from November 2020 to April 2021 has been plotted in Figure 1A.

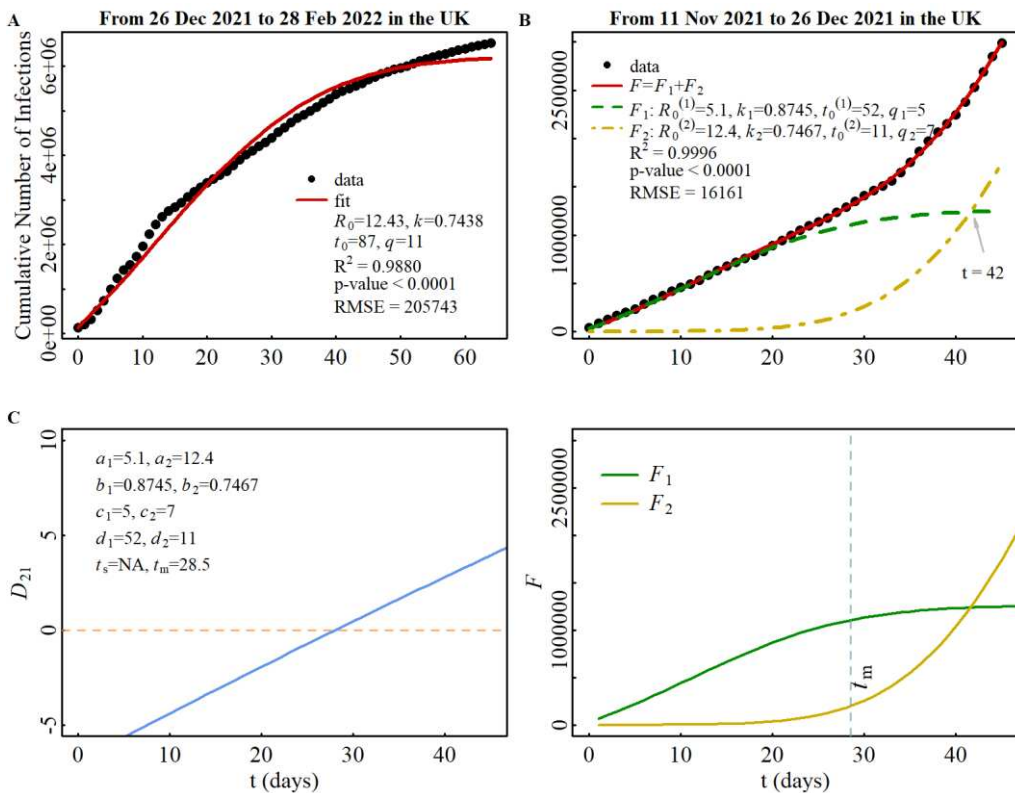


Figure 5. CNI simulation in the UK from November 2021 to February 2022. Panel A: CNI simulation of omicron spread in stage E (only the data of first omicron peak is used.); panel B: CNI simulation of delta/omicron spread in stage D; and panel C: Discriminant function and intersection of delta/omicron spread in stage D (left panel gives discriminant function and right panel the cross-spread of two strains).

4. Discussion

4.1. On the simulation of COVID-19 cases

The traditional SIR-type epidemic models depict the exponential growth of the number of infected individuals. However, empirical data has demonstrated that COVID-19 outbreaks do not exhibit exponential growth, but rather follow a three-parameter Gompertz growth function [10,11]. A new compartment model, known as the broken link model, has been proposed in the literature to explain the mechanism of Gompertz growth [12]. In our proposed model, we suggest that the spread of the virus depends on four parameters: R_0 , k , q and t_0 . R_0 describes the inherent infectious ability of the virus, k represents the strictness of social management, q represents the time needed for one step of infection, and t_0 is an additional parameter that aligns with the starting date of the experimental data. By incorporating these four parameters, our four-parameter simulation accurately fits all COVID-19 epidemic data involving a single strain of the virus. Consequently, the mechanism of Gompertz growth has been elucidated by our model and contributes to the prediction of future outbreaks.

4.2. On the mutation of the SARS-CoV-2 virus

The SARS-CoV-2 virus continuously undergoes mutations, giving rise to new strains. This ongoing mutation process is the reason why the pandemic has persisted for more than three years. As a result of natural selection, these new mutant strains possess higher infectious ability but lower lethality rates. Although the lethality rate of the new strains may be lower, it still results in a significant number of deaths. Therefore, since mutation occurrence is inevitable and costly, the key focus should be on reducing the epidemic probability of mutants. While humans cannot prevent the virus from mutating, they can hinder the mutant strains from dominating the competition. According to six prediction rules on cross-spread of two strains, it is highly unlikely for the intersection point t_{cr} to manifest under the following conditions: 1. when $\Delta > 0$, there are three domains and in this case there will be no occurrence of t_{cr} within a domain if the period of this domain is short enough (i.e. $t_s - t_a$ small, Δ small, or t_m large) or if the symbol of D_{21} within a domain does not align with the symbol of F_1-F_2 at the initial time of this domain; 2. when $\Delta < 0$, there is only one domain and in this case there will be no t_{cr} if the period of virus spread is short enough or if the symbol of D_{21} does not align with the symbol of F_1-F_2 at the initial time.

An example to highlight the phenomenon of no occurrence of t_{cr} is the winter epidemic in China in 2022. Among tens of millions of SARS-CoV-2 cases in one city, no new mutant strain emerged or triumphed over the competition, with the exception of the original omicron strand. This suggests that the pandemic was effectively terminated within a short period, lasting only one month.

In conclusion, the strategies proposed by our model to control an epidemic have two main aspects. First, it is critical to prevent the occurrence of a second wave. Second, one should aim to avoid competition among mutant strains. In the latter scenario, minimizing the duration of virus spread is an efficient approach.

4.3. Dependence of virus infection potential on temperature and humidity

The conformational equilibrium between the open and closed conformations of the receptor binding domain (RBD) of the spike (S) protein can be analyzed using first-principle techniques for a susceptible individual. The RBD can exist in either the open or closed position, known as the up or down conformation, respectively. The population of conformational states can be determined based on the free energy change during conformational transitions of the S protein. Let us denote the closed

conformation as state A and the open conformation as state B. The Gibbs free energies of states A and B are represented by G_A and G_B , respectively. Generally, if G_A is lower than G_B , the RBD will primarily assume the inactive conformation A. Conversely, in order to initiate the infectious process, the equilibrium should shift towards the open conformation, implying that G_B should be lower than G_A [13]. The free energy G in a given conformation is related to the partition function Z , which can be expressed as follows:

$$G = -k_B T \ln Z, \quad Z = \sum_n e^{-\beta E_n} \quad (\beta = \frac{1}{k_B T}). \quad (12)$$

Here E_n represents the energy level of a given conformation,

$$(E_n)_{A,B} = V_{A,B} + (n + 1/2)\hbar\omega_{A,B}, \quad (13)$$

$V_{A,B}$ represents two minima of conformational potential respectively and $(n+1/2)\hbar\omega_{A,B}$ the corresponding vibrational energy around the minimum of conformational potential. By the summation of Boltzmann factor over vibration states one has

$$\frac{Z_A}{Z_B} = e^{-\beta(V_A - V_B)} Y_{A/B}, \quad Y_{A/B} = \frac{e^{\frac{1}{2}\beta\hbar\omega_B} - e^{-\frac{1}{2}\beta\hbar\omega_B}}{e^{\frac{1}{2}\beta\hbar\omega_A} - e^{-\frac{1}{2}\beta\hbar\omega_A}}. \quad (14)$$

Let T_C represent the phase transition temperature, which can be determined by $\Delta G = G_B - G_A = 0$. From Eqs (12) and (14) we obtain a simplified equation for T_C

$$\frac{2(V_B - V_A)}{\hbar(\omega_A - \omega_B)} = \coth \frac{\hbar\omega_A}{2k_B T_C} \quad (\text{as } \left| \frac{\omega_A - \omega_B}{\omega_A} \right| \ll 1), \quad (15)$$

and $\Delta G > 0$ for $T > T_C$, $\Delta G < 0$ for $T < T_C$. Therefore, if the environmental temperature decreases to $T < T_C$, the conformational transition from the closed conformation to the open conformation occurs rapidly. This explains why the virus has higher transmission rates during the winter and the entrance to host cells is prioritized. Conversely, the summer season provides the most favorable conditions for virus elimination. In addition to temperature, the conformational equilibrium is influenced by humidity. The virus can be modeled as a charged sphere, and through the application of electrostatics principles to salty solutions, one can derive an expression for the potential at the surface of the charged sphere, where the dielectric constant ϵ is incorporated [14]. This implies that the elastic frequency ω^2 should be replaced by ω^2/ϵ . Considering water has a dielectric constant of $\epsilon=80$, the frequency parameter takes a reduced value of $\omega/9$ in the presence of a fully salty solution rather than ω in a vacuum. Consequently, this provides a quantitative estimation of the virus's infection potential, which is strongly dependent on humidity.

The above discussions on the susceptible individual can be extended to the population level, providing evidence that R_0 is influenced by temperature and humidity.

Author Contributions: Conceptualization, L.L.; validation, J.L., and L.L.; investigation, J.L.; writing—original draft preparation, L.L.; writing—review and editing, J.L.; visualization, J.L.; supervision, L.L. All authors have read and agreed to the published version of the manuscript.

Funding: This research received no external funding.

Institutional Review Board Statement: Not applicable.

Informed Consent Statement: Not applicable.

Data Availability Statement: Not applicable.

Conflicts of Interest: The authors declare no conflict of interest.

References

1. Kermack, W.O.; McKendrick, A.G. A contribution to the mathematical theory of epidemics. *Proc. R. Soc. Lond. A* **1927**, *115*, 700-721. doi: 10.1098/rspa.1927.0118
2. Murray, J.D. *Mathematical biology*, 2nd ed.; Springer-Verlag Berlin Heidelberg GmbH: New York, USA, 1993; pp. 1-92. doi: 10.1007/978-3-662-08542-4
3. Squazzoni, F.; Polhill, J.G.; Edmonds, B.; Ahrweiler, P.; Antosz, P.; Scholz, G.; Chappin, E.; Borit, M.; Verhagen, H.; Giardini, F.; et al. Computational models that matter during a global pandemic outbreak: A call to action. *JASSS* **2020**, *23*, 10. doi: 10.18564/jasss.4298
4. Adam, D. Special report: The simulations driving the world's response to COVID-19. *Nature* **2020**, *580*, 316-318. doi: 10.1038/d41586-020-01003-6
5. Sridhar, D.; Majumder, M.S. Modelling the pandemic. *BMJ* **2020**, *369*, m1567. doi: 10.1136/bmj.m1567
6. Parshani, R.; Carmi, S.; Havlin, S. Epidemic threshold for the susceptible-infectious-susceptible model on random networks. *Phys. Rev. Lett.* **2010**, *104*, 258701. doi: 10.1103/PhysRevLett.104.258701
7. Valdez, L.D.; Braunstein, L.A.; Havlin, S. Epidemic spreading on modular networks: The fear to declare a pandemic. *Phys. Rev. E* **2020**, *101*, 032309. doi: 10.1103/PhysRevE.101.032309
8. Wan, S.; Liu, J.; Liu, M. Progress on the basic reproduction number of SARS-CoV-2. *Chin. Sci. Bull.* **2020**, *65*, 2334-2341. doi: 10.1360/TB-2020-0413
9. Costris-Vas, C.; Schwartz, E.J.; Smith, R. Predicting COVID-19 using past pandemics as a guide: how reliable were mathematical models then, and how reliable will they be now? *Math. Biosci. Eng.* **2020**, *17*, 7502-7518. doi: 10.3934/mbe.2020383
10. Levitt, M.; Scaiewicz, A.; Zonta, F. Predicting the trajectory of any COVID19 epidemic from the best straight line. *MedRxiv* **2020**. Available online: <https://doi.org/10.1101/2020.06.26.20140814>.
11. Ohnishi, A.; Namekawa, Y.; Fukui, T. Universality in COVID-19 spread in view of the Gompertz function. *Prog. Theor. Exp. Phys.* **2020**, *12*, 123J01. doi: 10.1093/ptep/ptaa148
12. Ikeda, Y.; Sasaki, K.; Nakano, T. A new compartment model of COVID-19 transmission: The broken-link model. *Int. J. Environ. Res. Public. Health* **2022**, *19*, 6864. doi: 10.3390/ijerph1911686
13. Luo, L.F.; Zuo, Y.C. Spike conformation transition in SARS-CoV-2 infection. ArXiv 2021. Available online: <https://arxiv.org/abs/2009.11288v2>
14. Phillips, R.; Kondev, J.; Theriot, J.; Garcia, H.G. *Physical Biology of the Cell*, 2nd ed.; Garland Science: New York, USA, 2012; pp. 355-382.

Disclaimer/Publisher's Note: The statements, opinions and data contained in all publications are solely those of the individual author(s) and contributor(s) and not of MDPI and/or the editor(s). MDPI and/or the editor(s) disclaim responsibility for any injury to people or property resulting from any ideas, methods, instructions or products referred to in the content.